Criteria for discretization of seafloor bathymetry when using a stairstep approximation: Application to computation of T-phase seismograms

Catherine de Groot-Hedlin[a)]

Scripps Institution of Oceanography, UCSD, 8795 Biological Grade, La Jolla, California 92093-0225

Acoustic solutions for numerical models in which an overly coarse discretization of a stairstep boundary is employed to simulate smoothly varying bathymetry are degraded in a way that simulates scattering. Geometrical optics approximations are used to derive discretization criteria for simulating a smoothly sloping interface for the case of a source embedded in either an acoustic or an elastic seafloor, and applied to modeling T-phases. A finite difference time-domain modeling approach is used to synthesize T-phases for both smoothly sloping and rough seafloor boundaries. It is shown that scattering at a rough seafloor boundary yields ocean-borne acoustic phases with velocities near those of observed T-phase, while smooth seafloor models yield T-phases with slower horizontal velocities. The long duration of the computed T-phases for both the rough acoustic and elastic models is consistent with energy being scattered into the sound channel both as it transits the ocean/crust boundary, as well as at several subsequent seafloor reflections. However, comparison between the elastic and acoustic modeling solutions indicates that the T-phase wavetrain duration decreases with decreasing impedence contrast between the ocean and seafloor. © *2004 Acoustical Society of America.* [DOI: 10.1121/1.1643361]

I. INTRODUCTION

In many computational methods, a series of flat surfaces, or stairsteps, is used to represent a smooth, sloping boundary. Jensen (1998) demonstrated that the representation of sloping seafloor bathymetry by overly coarse stairsteps in ocean acoustic models leads to acoustic field solutions that include significant sidelobe diffractions. These numerical artifacts arise because each step acts as a point scatterer. If the spacing between stairsteps is a significant fraction of the incident wavelength for a source in the ocean column, the reflected phase consists of both a specularly reflected phase corresponding to the result for a smooth seafloor, and diffracted sidelobes resulting from coherent interference between waves diffracted from the array of point scatterers (Jensen, 1998). For sufficiently small spacing between the steps, the solution for the faceted boundary approximation approaches that for the smooth boundary.

This paper addresses the question of how finely seafloor bathymetry must be discretized to accurately model T-phase excitation. T-phases are seismically excited acoustic waves that propagate in the oceanic low-velocity sound channel, known as the SOFAR channel. Ray theory predicts that, because of the high velocity constrast between the oceanic crust and the ocean, *P* waves excited by a source within the crust or upper mantle are refracted into acoustic waves that propagate nearly vertically within the ocean column. Two mechanisms, or some combination thereof (Park *et al.*, 2001), are commonly invoked to explain how crustal sources excite nearly horizontally propagating acoustic phases trapped within the SOFAR channel. These are downslope

propagation (Tolstoy and Ewing, 1950; Talandier and Okal, 1998), which predicts that repeated interactions with a sloping seafloor result in an almost horizontally propagating acoustic phase, and scattering from a rough seafloor (de Groot-Hedlin and Orcutt, 1999, 2001), which predicts that acoustic phases are excited in proportion to the acoustic model amplitude at the seafloor depth.

In order to develop the modeling capability to distinguish between these competing hypotheses, it is vital to eliminate numerical artifacts associated with an overly coarse discretization of the seafloor and thus ensure that only physically realistic acoustic phases are synthesized. In this paper, the stairstep spacing necessary to avoid diffracted sidelobes is examined for sources embedded within the oceanic crust. The results for a fluid–fluid interface, that is, neglecting shear (*S*) velocities in the crust, and for a fluid–elastic boundary, with nonzero shear velocities within the crust, are considered separately. The results are applied to the computation of T-phases to determine which of the two competing excitation mechanisms is dominant in their excitation.

II. DIFFRACTIONS AT A STAIRSTEP INTERFACE

A. Fluid–fluid boundary

If each stairstep acts as an omnidirectional scatterer, then diffraction lobes are generated by constructive interference between waves radiated from neighboring scatterers. The direction in which the sidelobes propagate can be deduced from physical and geometrical considerations, as in Jensen (1998). In the following, sidelobe propagation angles are derived for a plane wave incident from below on a sloping fluid–fluid interface represented by a series of stairsteps. Although the focus of this investigation is on the excitation
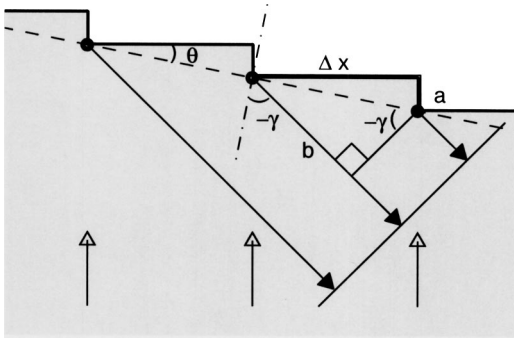
_____
[a)]Electronic mail: chedlin@ucsd.edu

FIG. 1. Diagram showing the geometry for computing the propagation angle of forward-reflected diffractions at a sloping boundary represented by stairsteps, for a plane wave incident directly from below. Coherent reflections occur when the stairstep spacing Δx is large enough that the difference in path length $(a+b)$ is an integral number of wavelengths. Diffraction angles are defined as positive clockwise from the normal to the interface.

of acoustic energy within the ocean, it is important to avoid creating reflected diffraction sidelobes within the seafloor, since reverberations within oceanic sediments or crustal layers can leak acoustic energy back into the seafloor. Therefore, discretization levels required to accurately model both seismic energy reflected back into the crust, and acoustic energy transmitted into the ocean column, are considered.

1. Reflected diffraction lobes

Consider a vertically propagating acoustic phase incident directly from below on an interface inclined downward to the right at an angle θ, represented by a series of stairsteps of height a located at intervals of Δx. The lower medium represents oceanic crust and sediments and the upper medium represents the ocean column. The angles at which forward-scattered diffraction lobes are reflected into the crust can be derived from the geometry shown in Fig. 1 (where forward is defined as the downslope direction). Constructive interference occurs at angles γ, for which the path difference $(a+b)$ is an integral number of wavelengths. Referring to Fig. 1, one obtains

$$\sin(-\gamma_n) = \frac{n\lambda_{\text{seis}}}{\Delta x}\cos(\theta) - \sin(\theta), \quad n=0,1,2,..., \quad (1)$$

where γ_n is defined as positive clockwise with respect to the normal to the interface, and λ_{seis} is the wavelength of the incident seismic wave. For $n=0$, this reduces to $\gamma_0 = \theta$, i.e., the angle of reflection is equal to the angle of incidence at a smooth interface. Thus, for a smooth interface modeled as a stairstep boundary, only the solution for $n=0$ is physically realistic and higher-order diffraction lobes are numerical artifacts.

The stairstep spacing necessary to eliminate these forward-reflected sidelobes may be derived from Eq. (1) as

$$\Delta x < \frac{\lambda_{\text{seis}}\cos(\theta)}{1+\sin(\theta)}. \quad (2)$$

Similarly, the angles at which backward-reflected diffraction lobes are generated can be derived as indicated in Fig. 2. This time, constructive interference occurs when the path length difference $(b-a)$ is an integral numbers of

wavelengths. Thus, diffraction lobes are generated at angles

$$\sin(\gamma_n) = \frac{n\lambda_{\text{seis}}}{\Delta x}\cos(\theta) + \sin(\theta), \quad n=0,1,2,.... \quad (3)$$

The solution for $n=0$ in Eq. (3) is identical to that of Eq. (1). The criterion for eliminating backscattered sidelobes is

$$\Delta x < \frac{\lambda_{\text{seis}}\cos(\theta)}{1-\sin(\theta)}. \quad (4)$$

Comparing Eqs. (2) and (4), it can be seen that the criterion for eliminating forward-reflected sidelobes is slightly more stringent than that for eliminating backscattered reflections. For the small-slope angles typical of the seafloor, the stairstep spacing need only be slightly smaller than the seismic wavelength.

2. Transmitted diffraction lobes

Derivation of the angles at which diffraction lobes are transmitted into the overlying medium is complicated by the fact that the wavelength of the acoustic phase excited in the ocean differs from that in the oceanic crust. As indicated in Fig. 3, these diffraction lobes are scattered forward at angles such that the path length difference $(a+b)$ is an integral number of wavelengths. Taking into account the difference in velocity, and hence wavelengths, between the crust and ocean, each path length may be written in terms of the fractional number of wavelengths, i.e., $a = \alpha\lambda_{\text{seis}}$ and $b = \beta\lambda_{\text{oc}}$,
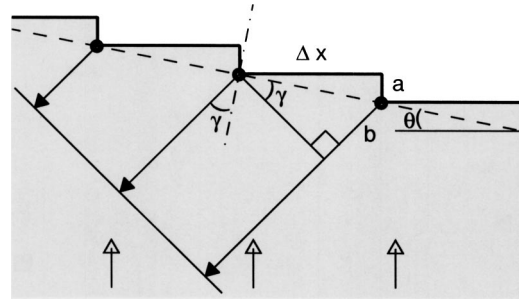

FIG. 2. Geometry for computing the propagation angle of upslope-reflected diffractions. Coherent reflections occur when the path length difference $(b-a)$ is an integral number of wavelengths. The solution for $b=a$ corresponds to specular reflection, and yields the physically realistic solution for a smooth boundary.
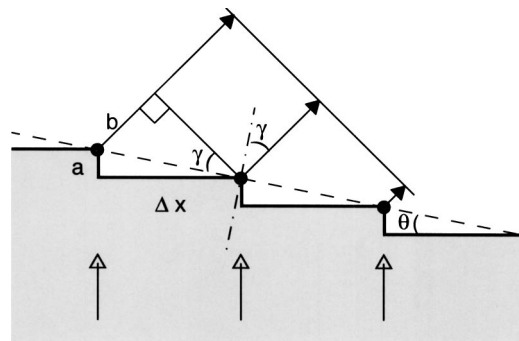

FIG. 3. Geometry for computing the propagation angle of diffractions transmitted into the ocean column in the downslope direction. Coherent reflections occur when the path length difference $(a+b)$ is an integral number of wavelengths.

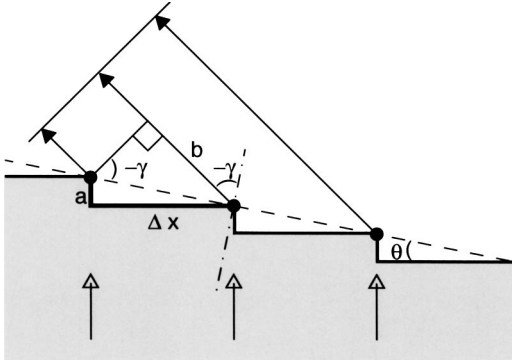Catherine de Groot-Hedlin: Criteria for discretization of seafloor bathymetry

FIG. 4. Geometry for computing the propagation angle of diffractions transmitted into the ocean column in the upslope direction. Coherent reflections occur when the path length difference $(b-a)$ is an integral number of wavelengths. The solution for $b=a$ yields Snell's law, and corresponds to the physically realistic solution for a smooth boundary.

where λ_{oc} is the acoustic wavelength within the ocean. Constructive interference occurs at angles such that $\alpha+\beta=n$, i.e.,

$$a+b=\alpha\lambda_{seis}+(n-\alpha)\lambda_{oc}. \quad (5)$$

Referring to the geometry of Fig. 3, one derives, after some algebraic manipulation

$$\sin(\gamma_n)=\frac{n\lambda_{oc}}{\Delta x}\cos(\theta)-\frac{v_{oc}}{v_{seis}}\sin(\theta), \quad n=0,1,2,..., \quad (6)$$

where v denotes velocity, and γ_n is the angle at which sidelobes are transmitted in the downslope direction, defined as positive clockwise with respect to the normal to the interface.

The solution for the fundamental lobe $n=0$ is just a statement of Snell's law (since γ_n is defined as positive clockwise from the normal to the interface) and is thus the physical solution for a smooth boundary. For $\theta=0$, Eq. (6) reduces to the equation for a diffraction grating (Halliday and Resnick, 1974); thus, higher-order lobes are numerical artifacts associated with overly coarse discretization of the boundary. From Eq. (6), it can be seen that a physically realistic solution is achieved given stairstep spacings of

$$\Delta x<\frac{\lambda_{oc}\cos(\theta)}{1+(v_{oc}/v_{seis})\sin(\theta)}. \quad (7)$$

Finally, diffraction lobes can be transmitted upslope into the overlying medium as shown in Fig. 4. Constructive interference occurs at angles for which the path length $(b-a)$ is an integer number of wavelengths. These angles are given by

$$\sin(-\gamma_n)=\frac{n\lambda_{oc}}{\Delta x}\cos(\theta)+\frac{v_{oc}}{v_{seis}}\sin(\theta), \quad n=0,1,2,...,$$
$$(8)$$

and sidelobe diffractions transmitted in the upslope direction are eliminated for

$$\Delta x<\frac{\lambda_{oc}\cos(\theta)}{1-(v_{oc}/v_{seis})\sin(\theta)}. \quad (9)$$

Given that acoustic velocities within the ocean column are usually lower than those of the crust, the criteria for

avoiding numerical artifacts associated with the stairstep approximation are not especially limiting. These criteria, given by Eqs. (2), (4), (7), and (9), indicate that for shallow slopes, the stairstep spacing must be slightly smaller than the smallest wavelength within the environmental model. For a typical ocean acoustic model, the ocean sound speed is less than that of the seafloor, so that Eq. (7) provides the limiting criterion for accurate solutions. As will be shown next, the introduction of shear velocities within the oceanic crust imposes stricter criteria on the stairstep spacing for a fluid–elastic boundary.

B. Fluid–elastic boundary

A multiplicity of phases can be excited at a fluid–elastic boundary. Compressional (P) waves incident on a smooth boundary can be reflected both as P- and S waves, and transmitted into the ocean as acoustic energy. Conversely, incident S waves give rise to reflected P- and S waves, as well as transmitted acoustic waves. For a stairstep boundary, each reflected and transmitted phase is potentially associated with diffracted lobes arising from an overly coarse discretization of the slope.

The criteria for ensuring that physically unrealistic sidelobes are not excited in the ocean column by a vertically propagating S wave incident on the solid–fluid interface are given by Eqs. (7) and (9), where v_{seis} is the S-wave velocity. Equations (2) and (4) hold for either P- to P-wave reflections or S- to S-wave reflections, where λ_{seis} is the appropriate seismic wavelength. The problem only becomes more complicated for P waves reflected into S-wave energy, or S waves reflected into P-wave energy within the solid. In this case, referring again to the geometry of Fig. 1, it can be seen that forward-scattered diffraction lobes are formed at angles

$$\sin(-\gamma_n)=\frac{n\lambda_{seis}^{out}}{\Delta x}\cos(\theta)-\frac{v_{seis}^{out}}{v_{seis}^{in}}\sin(\theta), \quad n=0,1,2,...,$$
$$(10)$$

where v_{seis}^{in} refers to the velocity of the vertically propagating wave incident on the interface and v_{seis}^{out} and λ_{seis}^{out} are the velocity and wavelength of the outgoing seismic phase, respectively. Again, the fundamental lobe solution ($n=0$) is the only physically realistic one. Thus, the required stairstep spacing is

$$\Delta x<\frac{\lambda_{seis}^{out}\cos(\theta)}{1+(v_{seis}^{out}/v_{seis}^{in})\sin(\theta)}. \quad (11)$$

Compressional velocities are always greater than shear velocities within an elastic solid, and in water-saturated sediments the ratio may be as high as 13 (Hamilton, 1979). Thus, for S- to P conversions, Eq. (11) predicts that the required stairstep spacing is very small. For a V_p/V_s ratio of 2, the required stairstep spacing is $\lambda_p/3$ for a 40° slope; for a V_p/V_s ratio of 10, a 40° stairstep slope must be sampled at intervals of $\lambda_p/10$. Corresponding discretization values for P- to S conversions are predicted to be even smaller. For $V_p/V_s=2$, Δx must be less than or equal to $0.55\lambda_s$ ($\approx\lambda_p/3.5$) for a 40° slope; for $V_p/V_s=10$, Δx must be less
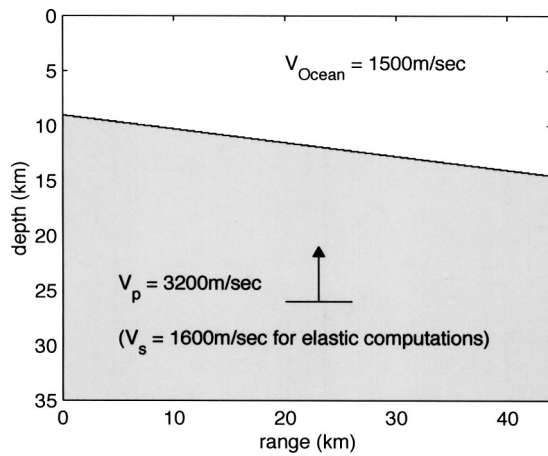
FIG. 5. Environmental model for numerical computations, with varying stairstep spacings. A cosine beam of width 6 km, at 26-km depth, is incident from below on a boundary with a 1:8 gradient. The compressional velocity is 3200 m/s in the lower medium and 1500 m/s in the upper medium. For the acoustic computations, the shear velocity is 0 throughout; for the elastic computations, the shear velocity is 1600 m/s in the lower medium.

FIG. 6. The source function for the computations. (a) Time series for the central element within the source beam. (b) The source spectrum.

than or equal to $0.7\lambda_s(\approx\lambda_p/14)$ for the same slope.

Similarly, the general formula for diffraction angles of backscattered reflections is given by

$$\sin(\gamma_n) = \frac{n\lambda_{seis}^{out}}{\Delta x}\cos(\theta) + \frac{v_{seis}^{out}}{v_{seis}^{in}}\sin(\theta), \quad n = 0,1,2,...,$$ (12)

and the appropriate discretization is

$$\Delta x < \frac{\lambda_{seis}^{out}\cos(\theta)}{1 - (v_{seis}^{out}/v_{seis}^{in})\sin(\theta)}.$$ (13)

The stairstep spacing required for accurately modeling backscattered reflections is larger than for the forward-scattered reflections. Thus, the limiting stairstep spacing required to simulate a smooth boundary when modeling seismic to acoustic interactions for sources within the elastic ocean crust is given by Eq. (11), for an incident P wave and a reflected S wave.

III. NUMERICAL SOLUTIONS

A. Results for a fluid–fluid boundary

The test problem, shown in Fig. 5, features an interface that angles downward to the right at a gradient of 1/8 ($\approx 7.1°$). The compressional velocity is 1.5 km/s in the upper medium and 3.2 km/s in the lower medium; the density contrast between the lower and upper medium is 2.3. The densities and compressional velocities of the lower medium are representative of solidified marine sediments at the ocean floor. Acoustic field solutions are sought for a compressional cosine source beam directed upward. Each element in the source array is a 5-Hz sinusoid with exponential growth and decay as shown in Fig. 6(a); the bandwidth of the source is as shown in Fig. 6(b).

The criteria developed in the previous section are valid for monochromatic plane waves incident on a stairstep boundary from directly below; however, the cosine beam
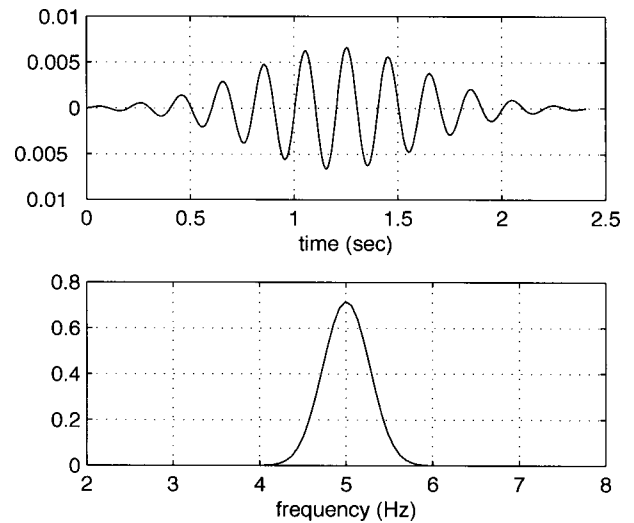
source used here is neither perfectly planar nor monochromatic. Given that the source beam has a finite width and is located a finite distance from the stairstep boundary, it may be mathematically represented as a superposition of plane waves using the Cagnaird–de Hoop method (Aki and Richards, 1980), with wave vectors pointing in all directions. The presence of energy with wave vectors in a direction that departs from that of the main beam affects the stepsize criterion; the geometry for forward scattering from a beam incident at an arbitrary angle i with respect to the normal to a stairstep boundary is shown in Fig. 7. As before, the path lengths d and b may be written in terms of the fractional number of wavelengths, i.e., $d = \alpha\lambda_{seis}$ and $b = \beta\lambda_{oc}$. Constructive interference occurs at angles such that $\alpha + \beta = n$. After some algebraic manipulation, one derives

$$\sin(\gamma_n) = \frac{n\lambda_{oc}}{\Delta x}\cos(\theta) - \frac{v_{oc}}{v_{seis}}\sin(i), \quad n = 0,1,2,..., \quad (14)$$

as the angles at which constructive interference occurs. Again, only the $n = 0$ solution is physically realistic, so the stairstep discretization criterion for a plane wave incident at
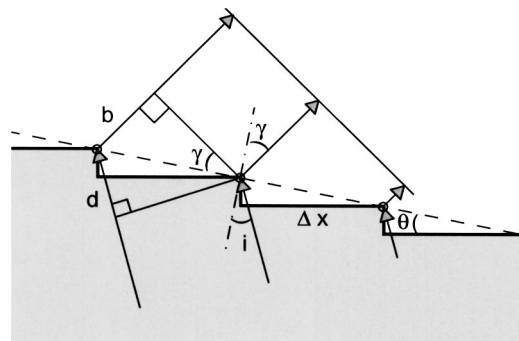

FIG. 7. Geometry for computing the propagation angle of diffractions transmitted into the ocean column in the downslope direction for a plane source at an incidence angle of i with respect to the boundary. Coherent reflections occur when the path length difference $(d+b)$ is an integral number of wavelengths.

Catherine de Groot-Hedlin: Criteria for discretization of seafloor bathymetry

an arbitrary angle i with respect to the normal to the interface becomes

$$\Delta x < \frac{\lambda_{oc} \cos(\theta)}{1 + (v_{oc}/v_{seis})\sin(i)}. \tag{15}$$

It may be similarly shown that the $\sin(\theta)$ term in the denominator of each of the discretization criteria listed in Eqs. (2), (4), (9), (11), and (13) is replaced by $\sin(i)$. Thus, given that the discretization criteria depend on both the angle of incidence and the frequency (through the wavelength), it should be emphasized that they do not represent a sharp cutoff, but rather, the onset of scattering is gradual. A broader discussion on the use of beams to approximate a plane wave source may be found in Stephen (2000).

Finally, interface waves, like head waves or Stoneley waves, which are excited by the interaction of a spherical wave with a plane boundary, could be excited by the source beam since it includes spherical wave components. Furthermore, since the stairsteps act as secondary point scatterers, they could also play a role in exciting interface waves. A full treatment of interface waves is beyond the scope of this paper; however, in the examples shown here, the solutions are dominated by the diffraction effects discussed in the previous section.

A two-dimensional (2D) acoustic finite difference time-domain (FDTD) modeling method is applied to the test problem. To eliminate reflections from outgoing waves at the edges of the computational domain, and thereby model an unbounded region, the perfectly matched layer absorbing boundary condition (Berenger, 1994), modified for use in acoustics, is used to absorb energy at the bottom and sides of the grid over a wide range of angles. For each computation, a grid spacing of 20 m in both the horizontal and vertical directions is used, i.e., over 15 points per compressional wavelength—greater than the minimum of 10–12 nodes per wavelength required to minimize numerical dispersion in the FDTD approach (Taflove and Hagness, 2000). In the following, acoustic field solutions are computed for a series of stairstep spacings in increments of 160 m. These spacings were chosen so that the grid size could be uniform within each model. Thus, for a stairstep spacing of 160 m, a vertical step of 1 gridpoint occurs every 8 horizontal gridpoints; for a stairstep spacing of 320 m, a vertical step of 2 gridpoints occurs every 16 horizontal gridpoints, etc., given that the slope has an average gradient of 1/8. Thus, differences in the solutions are due to variations in both the stairstep spacing and the step rise. Larger rises between steps mainly affect the amplitude of the sidelobes; however, an examination of the sidelobe amplitudes is beyond the scope of this paper.

Equation (7) predicts that the maximum allowable spacing required for modeling physically realistic transmissions at the seafloor boundary is 281 m for a 5-Hz source. The acoustic field solution for a model with a stairstep spacing of 160 m, shown in Fig. 8 at $t = 11.25$ s, thus corresponds to the result for a smooth slope. By this time, the upgoing acoustic phase has been partly reflected from the interface at an angle of 2θ with respect to the incident phase, and partly transmitted into the upper medium in a direction nearly perpendicular to the interface, as predicted by Snell's law.
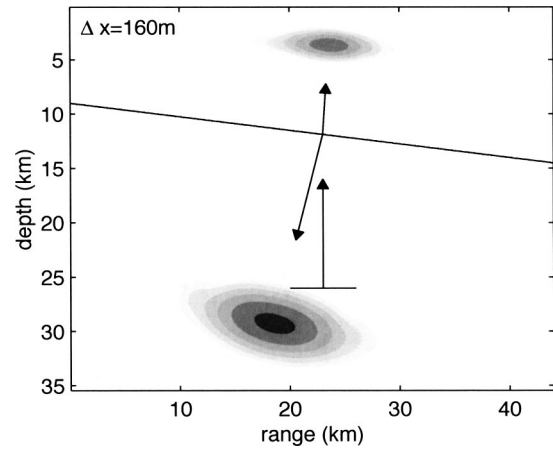

FIG. 8. Envelope of the acoustic field solution for a stairstep spacing of 160 m. The result corresponds to that of a smooth sloping boundary. Arrows show the direction of the incoming phase and the predicted angles of specular transmission and reflection for $f = 5$ Hz. The length of each arrow is proportional to the velocity of the phase. Contour intervals are from 24 to 60 dB (from white to black), in steps of 6 dB.

Figure 9 shows acoustic field solutions at $t = 11.25$ s, computed at stairstep spacings of 320 m and more. Equations (7) and (9) predict that diffraction sidelobes are transmitted in both the upslope and downslope directions for $\Delta x = 320$ m, but that no sidelobes should be excited in the lower medium at this spacing. This is confirmed by Fig. 9(a); diffraction sidelobes excited in the ocean propagate at angles of approximately 61° with respect to the normal in the downslope direction and 81° in the upslope direction, as predicted by Eqs. (6) and (8), respectively. As shown in the lower panels, the angle of propagation of these numerical artifacts steepens with increasing stairstep spacing. This is in agreement with the predicted propagation angles, which are shown by the arrows in each panel.

With stairstep spacings greater than 540 m, sidelobes corresponding to both the $n = 1$ and $n = 2$ solutions of Eqs. (6) and (8) are transmitted into the ocean column. Although a full analysis of the diffraction amplitudes is beyond the scope of this paper, note that Fig. 9 indicates that the amplitude of the sidelobes decreases with increasing order number, similar to the behavior of a diffraction grating. As the stairstep spacing increases beyond 565 m, Eq. (2) predicts that forward-reflected sidelobes are generated in the lower medium, as shown in Fig. 9(c). For stairstep spacings greater than 725 m, sidelobes are also reflected in the upslope direction, as shown in Fig. 9(d), and as predicted by Eq. (4). Figure 9(d) also shows a third-order diffraction node in the ocean that, from Eq. (6) should not exist for $f = 5$ Hz. The existence of this sidelobe is likely due to the source bandwidth; third-order sidelobes can be generated in the downslope direction for $f > 5.3$ Hz, which is within the source bandwidth as shown in Fig. 6(b).

B. Results for a fluid–solid boundary

The test problem is similar to that described above for a fluid–fluid boundary, with the exception that the lower medium in this case is an elastic solid with a shear velocity of 1.6 km/s. A 2D FDTD method suitable for elastic media
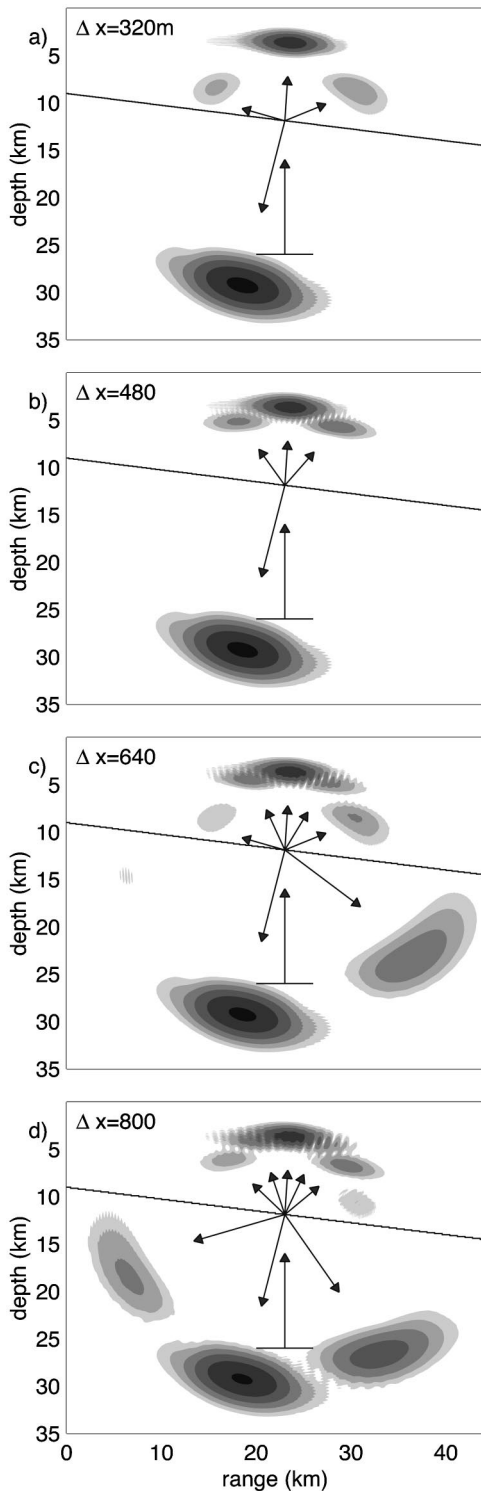
FIG. 9. Acoustic field solutions for stairstep spacings of (a) 320 m; (b) 480 m; (c) 640 m; and (d) 800 m. Arrows show the predicted propagation directions of both the specular and diffracted phases.

(Virieux, 1986), is applied to the test problem. A first-order absorbing boundary condition is used to terminate the sides and bottom of the grid to simulate an infinite half-space (e.g., Taflove and Hagness, 2000). As before, a grid spacing of 20 m in both the x and z directions is used. Again, a pressure source beam with a center frequency of 5 Hz is applied. However, because the source lies within the elastic medium, it is impossible to introduce an entirely compressional source

beam. Instead, the differential pressure at the edges of the beam yields a small shear source component with a velocity equal to that of the compressional beam. The derived solutions are thus a superposition of the results for both a compressional source and a shear source.

For this problem, the maximum allowable spacing for avoiding physically unrealistic diffractions is identical to that of the acoustic problem above, i.e., 281 m. The elastic solution for a model with a stairstep spacing of 160 m is shown in Fig. 10, at 11.25 s. The pressure field, shown in Fig. 10(a), is nearly identical to the acoustic field solution shown in Fig. 8. The shear field solution, shown in Fig. 10(b), features two reflected waves. The faster one is an artifact arising from the fact that the source beam includes both shear and compressional components, which propagate at equal velocity. The incident shear component gives rise to the faster, specularly reflected shear phase. The slower reflected phase is associated with the partial reflection of the incident P wave into an S wave.

Figure 11 shows the pressure field solution and the shear stress field for a stairstep spacing of 320 m. The pressure field is nearly identical to the acoustic field solution of Fig. 9(a). However, as shown in Fig. 11(b), shear diffractions are excited in the lower medium by the incident P phase. The sidelobe to the right propagates at the angle predicted by Eq. (10) for an incident P wave and outgoing shear diffracted phase, at 5 Hz. Equation (12) predicted that the shear sidelobe to the left should only exist at frequencies greater than 5.3 Hz; thus, its presence is likely due to the finite source bandwidth.

IV. MODELING T-PHASE EXCITATION

The examples of the previous section illustrate not only the limits that must be placed on the stairstep spacing in order to obtain a physically realistic solution but also, incidentally, the effectiveness of scattering from an array of point sources in transforming an upgoing seismic phase into a nearly horizontally propagating acoustic phase in the ocean column. Therefore, in a modeling study designed to distinguish between the two competing hypotheses of T-phase excitation, i.e., downslope propagation vs seafloor scattering, it is vital to limit the stairstep size in order to avoid introducing acoustic scattering artifacts that result only from an overly coarse discretization of the seafloor, and not from actual roughness in the model.

In computing T-phases, one must consider the multiple interactions of the ocean acoustic phase with the seafloor, as well as the upgoing seismic phase. In downslope propagation at a slope with angle θ, it can be shown that the propagation angle steepens by 2θ with each bottom interaction. For a plane wave with incident angle i with respect to the stairstep boundary, the spacing required to maintain accuracy in the downward reflected acoustic waves within the ocean column is

$$\Delta x < \frac{\lambda_{oc} \cos(\theta)}{1 - \sin(i)}, \tag{16}$$

where we have substituted λ_{oc} for λ_{seis} in Eq. (4)—because the geometry for propagation within the ocean is similar to

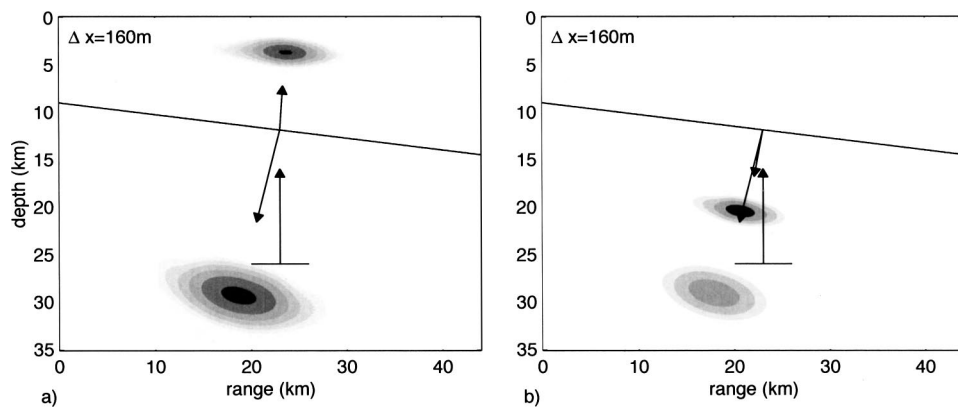Catherine de Groot-Hedlin: Criteria for discretization of seafloor bathymetry

a)

b)

FIG. 10. Solution for a stairstep spacing of 160 m. The pressure field is shown in (a). The shear field, represented by the stress tensor component τ_{xz}, is shown in (b). The result corresponds to the result for a smooth sloping boundary. The faster shear component excited in the lower medium is a source artifact arising from the fact that the compressional source beam generates a small shear component with equal velocity.

the geometry in Fig. 2, with the ocean and seafloor reversed—and $\sin(i)$ for $\sin(\theta)$—because, as outlined in Sec. III, the $\sin(\theta)$ term in the denominator of each discretization criterion in Sec. II is replaced by $\sin(i)$ for an arbitrary angle of incidence i. Thus, the criterion for simulating a smooth interface becomes less stringent with repeated seafloor reflections, that is, Δx increases as the propagation angle inclines to the horizontal.

In this section, T-phase excitation is computed for several versions of a 2D model with a simple triangular ridge, as shown in Fig. 12. In each one, the water velocity profile corresponds to the annual average sound-speed profile at (42N,130W), as derived from the Levitus database (Levitus and Boyer, 1994). The seafloor velocity profile consists of two layers representing the upper and middle oceanic crust, with velocities and thicknesses obtained from the CRUST2 model at 43N, 129W. (The CRUST2 model is available at http://mahi.ucsd.edu/Gabi/rem.html) The model features a ridge with sides sloping at angles of 6.8°, with a peak at 1.5-km depth, well below the sound-speed minimum at 575 m but above the reciprocal depth at 2.8 km. The source is a point source located at 7-km total depth, directly below the peak of the ridge. The source time function and spectrum are as shown in Fig. 6. Responses are synthesized for a vertical array of hydrophones at depths from 50 to 2950 m at a 50-m spacing, at a lateral distance of 100 km from the source, and also for a horizontal "array" at the depth of the sound-speed minimum, 600 m, at ranges from 20 to 110 km from the ridge peak, with a lateral spacing of 10 km.

T-phases are calculated for four variants of the model using the time-domain finite difference methods described in

the previous section. The object is to determine the role that small-scale seafloor roughness plays in exciting T-phases, and also to examine the importance of treating the oceanic crust and sediments as elastic materials. The first variation is an acoustic model, that is, the shear velocities are identically zero, and the seafloor and sides of the ridge are modeled as flat surfaces. The stairstep spacing for the sides of the ridge ranges from 200 to 225 m, below the minimum spacing of 240 m needed to simulate a smooth, sloping interface, as derived by Eq. (7) for a source with a maximum frequency of 6 Hz. Note that seafloor roughness has not been entirely eliminated as the ridge peak serves as a large scale scatterer. For the second set of computations, the top of each layer is replaced by a rough surface, as indicated by the heavy lines shown in Fig. 12. The scale of the seafloor roughness is within the limits imposed for small-scale scattering, i.e., the amplitude of the scatterers is smaller than the source wavelength, and the gradient is much less than 1 (Ogilvy, 1987). For the third model, the seafloor is an elastic medium with velocities as given in Fig. 12, with smooth sides. For this model, the minimum stairstep spacing required to simulate smooth sides is 231 m, as given by Eq. (7) for an incident 6-Hz S wave with velocity 2.5 km/s. The final model is an elastic model with the top oceanic crustal boundaries replaced by a rough surface.

The models differ from realistic ocean models in several important respects. First, the real seafloor is generally characterized by roughness over a wide range of scale lengths (Herzfeld et al., 1995). Here, the treatment of seafloor roughness is limited to small-scale scattering. In most regions where submarine earthquakes occur, the seafloor is rougher
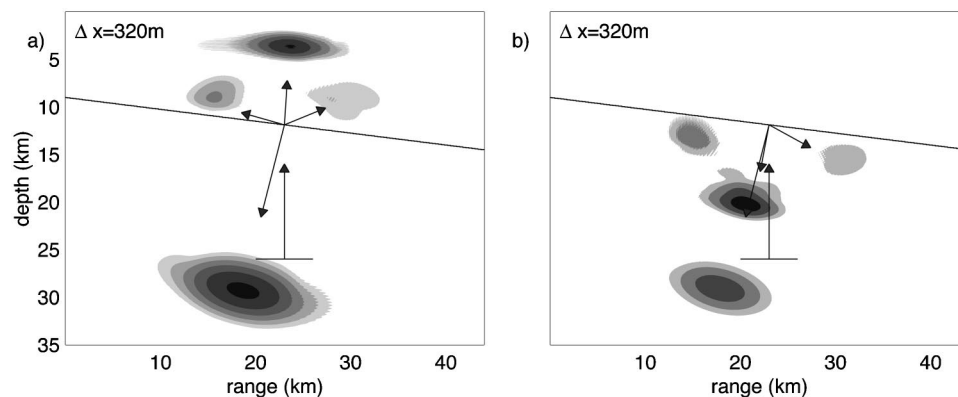

a)

b)

FIG. 11. Elastic field solutions. (a) pressure field for $\Delta x = 320$ m; (b) shear field for $\Delta x = 320$ m.
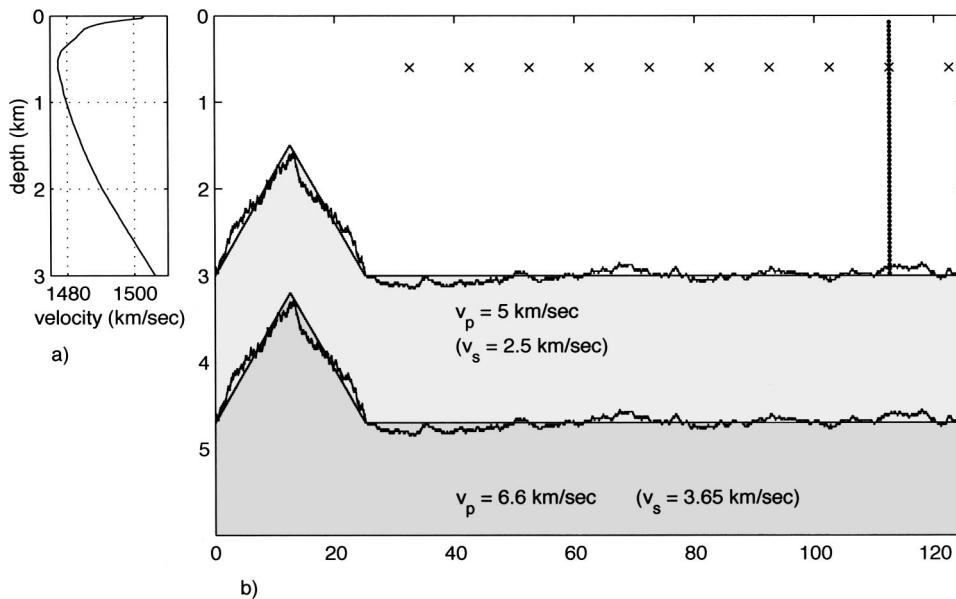
FIG. 12. Environmental model for numerical computation of T-phases. The model consists of 5000×360 elements, each 25 m on a side. Slopes are modeled using a stairstep approximation. A vertical hydrophone array consisting of 59 elements at depths ranging from 50 m to 1 km is located 100 km from the ridge. The locations of hydrophones at the sound-speed minimum are marked by x's. The ocean sound-speed profile is shown to the left. The seafloor velocities are typical for seafloor crust.

than the models. Second, low-velocity marine sediments are not included in any of the models, although they may play an important part in T-phase excitation and propagation (de Groot-Hedlin and Orcutt, 2001). Soft sediments are neglected here due to numerical constraints; the very fine discretization required to include a layer with very low shear velocities would make the problem too computationally intensive. Finally, attenuation within the seafloor is neglected in these models.

A. Acoustic solution

The critical angle for ocean/crust reflection is only 17.5° with respect to the normal to the seafloor boundary for the acoustic models. Given that the slope angle of the ridge is 6.8°, only one or two downslope reflections of the acoustic phase at the sloping seafloor are needed to trap the acoustic phase within the ocean layer. By contrast, an acoustic phase would have to propagate at an angle of 79° with respect to the vertical to be completely trapped within the sound channel for the given ocean velocity profile. That would require six downslope reflections at the sloping boundary. A phase

propagating at the critical angle would be multiply reflected from both the sea surface and seafloor and have a horizontal velocity of 450 m/s. This would be the slowest velocity at which one could expect to see any arrivals. Oceanic phases with a greater number of reflections at the sloping ridge would yield a phase propagating at an angle inclined further to the horizontal, with earlier arrivals. More steeply propagating phases would have a slower phase velocity and would be eventually transmitted into the seafloor.

Figure 13 shows smoothed envelopes of the pressure responses for the acoustic model along the line of hydrophones at 600 m. Envelopes are plotted since phase information at this distance is inaccurate due to the numerical dispersion inherent in the FDTD method (Taflove and Hagness, 2000). The dash-dotted line corresponds to arrivals with a group velocity of 1.5 km/s, i.e., a T-phase. The dashed line corresponds to arrival times for a phase propagating at the critical angle to the interface. The large-amplitude arrivals for the model with smooth seafloor planes, shown in Fig. 13(a), propagate at about 1.1 km/s across the array. The lack of energy at T-phase velocities indicates that little energy is
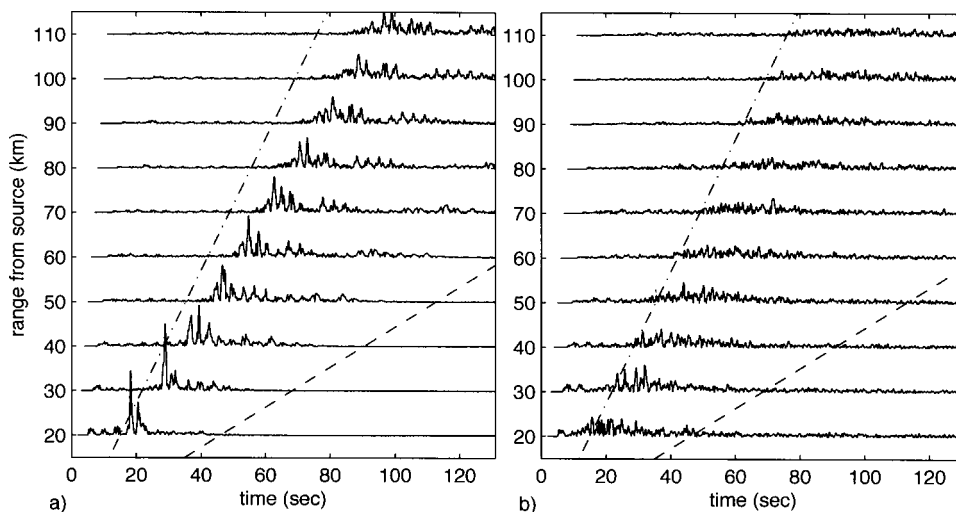

FIG. 13. Envelopes of the pressure responses at the horizontal hydrophone array for the acoustic seafloor models. The dotted line corresponds to the expected T-phase arrival; the dashed line corresponds to an arrival for an acoustic phase propagating at the critical angle to the seafloor. (a) Acoustic field solution for the smooth seafloor model. (b) Acoustic field solution for the rough seafloor. Amplitudes scales are uniform for (a) and (b).
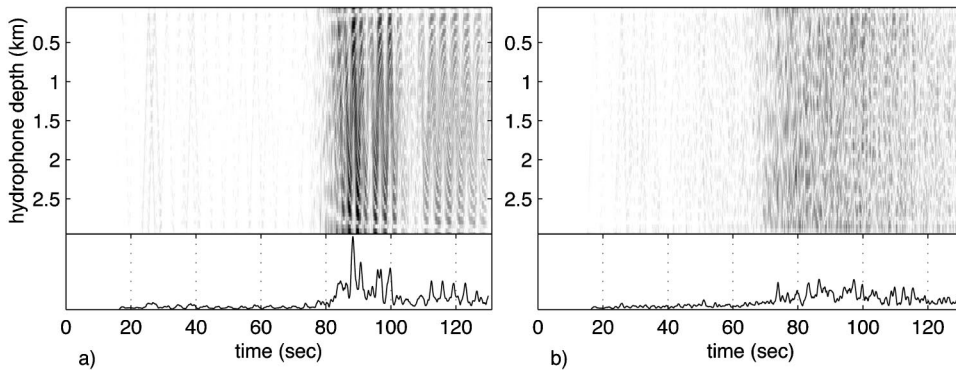
FIG. 14. Envelopes of the pressure response at the vertical hydrophone array for the acoustic seafloor models. Envelopes for the element at the sound-speed minimum, smoothed over 0.75 s, are shown below the array response for each example. (a) Acoustic field solution for smooth seafloor model. (b) Acoustic field solution for the rough seafloor.

scattered directly into the sound channel by the ridge peak. Corresponding results for the model with the rough seafloor, in Fig. 13(b), show that the earliest arriving ocean-borne acoustic phases propagate at the T-phase velocity. These would correspond to energy scattered directly into the sound channel nearest the ridge peak. The length of the wavetrain indicates that acoustic energy is scattered into the sound channel at several subsequent seafloor reflections. Although the maximum amplitude of the arrivals for the smooth seafloor model are 2–3 times greater than for the rough model, they decrease more rapidly with increasing range from the ridge.

Figure 14 shows pressure envelopes for the vertical hydrophone array at a range of 100 km from the ridge peak for each of the acoustic models, along with the smoothed envelope for the element at 600 m, near the sound-speed minimum. The results for the smooth seafloor model (left) clearly indicate that the arrivals are reflections between the ocean surface and seafloor, whereas distinct reflections are not observed in the corresponding acoustic phases for the rough seafloor model (right). Pressure amplitudes are significant below the reciprocal depths for both models.

B. Elastic solutions

The critical angle for ocean/crust reflection increases when shear velocities are introduced. For the model of Fig. 12, it is 36.9°; thus, at least three downslope reflections are required to trap acoustic energy within the ocean. Since there

is bottom loss at each downslope reflection before the critical angle is reached, the amplitude of the trapped acoustic phase is expected to be lower than for the corresponding acoustic model. Acoustic phases propagating at the critical angle would have a horizontal velocity of 1.125 km/s.

The pressure responses along the horizontal hydrophone array are shown in Fig. 15 for the model with the elastic seafloor. The dashed line corresponds to arrivals with the horizontal velocity of a phase propagating at the critical angle for shear waves. The later arrivals for the smooth seafloor, shown in Fig. 15(a), propagate more steeply than the critical angle and so should eventually be transmitted into the seafloor at greater ranges. As expected, the amplitude of the trapped acoustic phase is much smaller than for the corresponding model with the fluid seafloor—note that the initial P waves can be seen at this scale. Overall, the waveforms are shorter in duration but more complex than for the corresponding acoustic models.

Envelopes of the pressure responses at the vertical hydrophone array are shown in Fig. 16. Again, distinct reflections are observed in the results for the smooth seafloor but not for the rough seafloor. A faint reflection at about 60 s for the smooth seafloor model corresponds to an arrival that is trapped between the ocean surface and lower crust layer. The peak amplitudes for the rough model arrive nearly 20 s before those of the corresponding smooth seafloor model, indicating that the trapped acoustic phases propagate more horizontally for the rough seafloor model. Again, this implies
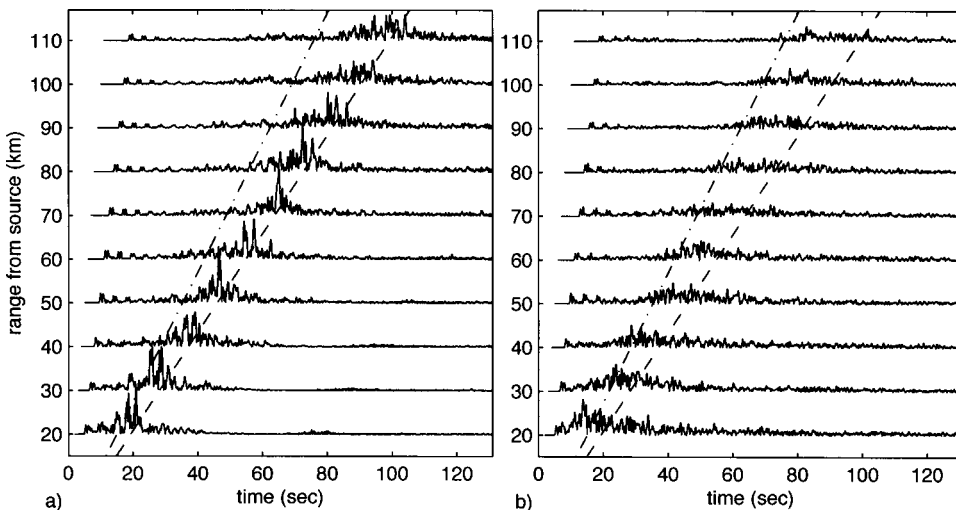

FIG. 15. Similar to Fig. 13, but for the elastic seafloor models. Amplitude scales are uniform for (a) and (b).
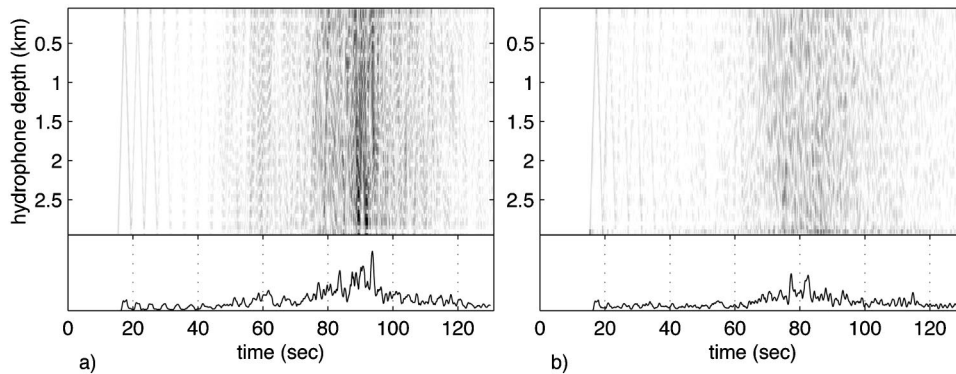
FIG. 16. Similar to Fig. 14, but for the elastic seafloor models.

that small-scale roughness at the seafloor is an effective mechanism for converting vertically propagating seismic energy into a nearly horizontally propagating T-phase.

V. DISCUSSION

The discretization criteria developed in Sec. II indicate that the stairstep spacing required to simulate a smooth slope decreases with increasing slope angle. However, numerical computation of T-phases generated at low slope angles may be equally problematic since, for any numerical method in which sloping boundaries are represented by stairsteps, the distance between steps increases with decreasing slope angle. Given that downward propagation at a shallow slope is relatively inefficient at converting a vertically propagating acoustic phase to a nearly horizontally propagating phase (since bottom loss is high at near-vertical incidence), the energy contributed by sidelobe diffractions may actually dominate the computed acoustic arrivals at large distances.

Reliable synthesis of T-phases requires accuracy over a wide range of directions, from upgoing seismic phases to horizontally propagating ocean acoustic phases. This is in contrast to the case for a source within the ocean column, where one may usually neglect vertical propagation for long-range propagation problems. Thus, a more efficient and accurate method of computing T-phases would be to employ a two-stage process. In the vicinity of the source region, a computational method that is accurate over all propagation directions would be applied, using small step sizes. As the ocean acoustic phase inclines to the horizontal at greater ranges from the source, a more efficient computational method that is accurate at larger step sizes could be used.

VI. CONCLUSIONS

Discretization levels necessary to simulate a smooth interface using a stairstep boundary were derived using a model of an incident plane wave on a sloping boundary with point scatterers arrayed along its length. The stairstep spacings needed to accurately compute both forward (downslope) and backward (upslope) sidelobe reflections and transmissions for both fluid–fluid and solid–fluid boundaries were found to be proportional to the smallest wavelength in the model. The results also indicate that the criterion for eliminating either forward-reflected or backward-transmitted sidelobes is the most stringent.

A modeling study was conducted to distinguish between the two competing hypotheses of T-phase excitation—downslope propagation and seafloor scattering—and to determine the importance of modeling the seafloor as an elastic medium. The models were discretized in accordance with the stairstep spacings derived earlier to ensure that any scattered energy in the acoustic field solutions resulted from real model roughness and was not a numerical modeling artifact. The results indicate that the acoustic phases trapped in the ocean column for the smooth models had higher amplitudes but lower velocities than for the corresponding rough models for ranges up to 110 km from the epicentral location. Given that the velocity of the trapped acoustic phase for the rough model is closer to that of observed T-phases (Tolstoy and Ewing, 1950) and that the roughness of the seafloor in the vicinity of most submarine earthquakes is actually greater than that of the rough models in this study (so that scattering would be even stronger), I conclude that scattering is the dominant mechanism for T-phase excitation, even in regions of high impedance contrast. If downslope propagation was the dominant mechanism, one would expect to observe much slower T-phase velocities. A much steeper feature would be required to generate downslope-generated acoustic phases with greater horizontal velocities. However, most observed T-phases are generated at bathymetric features no steeper than the ridge modeled here. The computed amplitudes for the smooth models may be unrealistically large because seafloor attenuation was neglected in each model.

The relatively long wavetrains of the trapped acoustic phases for both the rough acoustic and elastic models suggests that energy is scattered into the sound channel both as it transits the ocean/crust boundary, and at several subsequent seafloor reflections. This is in contrast to the model of T-phase excitation proposed by de Groot-Hedlin and Orcutt (2001), in which only primary scattering was considered and energy contributions by the ensuing seafloor reflections were neglected. That model proved adequate in regions with thick layers of gently sloping marine sediments. For a model with low-velocity marine sediments, much of the energy would be transmitted into the seafloor at each bottom reflection, so there would be little energy remaining to be scattered into the sound channel after the first reflection. This implies that T-phases should be longer for models with high impedance contrasts. This hypothesis is supported by the models considered in this paper; the effective impedance contrast between the ocean column and seafloor is greater for the model with

the acoustic seafloor than with the elastic seafloor (Brekhovskikh and Lysanov, 1991), and the computed wavetrains have greater durations for the acoustic than for the elastic seafloor model.

Aki, K., and Richards, P. G. (**1980**). *Quantitative Seismology: Theory and Methods* (Freeman, San Francisco).

Berenger, J.-P. (**1994**). "A perfectly matched layer for the absorption of electromagnetics waves," J. Comput. Phys. **114**, 185–200.

Brekhovskikh, L. M., and Lysanov, Y. P. (**1991**). *Fundamentals of Ocean Acoustics* (Springer, Berlin).

de Groot-Hedlin, C. D., and Orcutt, J. A. (**1999**). "Synthesis of earthquake-generated T-waves," Geophys. Res. Lett. **26**, 1227–1230.

de Groot-Hedlin, C. D., and Orcutt, J. A. (**2001**). "Excitation of T-phases by seafloor scattering," J. Acoust. Soc. Am. **109**, 1944–1954.

Halliday, D., and Resnick, R. (**1974**). *Fundamentals of Physics* (Wiley, Toronto).

Hamilton, E. L. (**1979**). "V_p/V_s and Poisson's ratios in marine sediments and rocks," J. Acoust. Soc. Am. **66**, 1093–1101.

Herzfeld, U. C., Kim, I. I., and Orcutt, J. A. (**1995**). "Is the ocean floor a fractal?," Math. Geol. **27**, 421–462.

Jensen, F. B. (**1998**). "On the use of stair steps to approximate bathymetry changes in ocean acoustic models," J. Acoust. Soc. Am. **104**, 1310–1315.

Levitus, and Boyer (**1994**). *World Ocean Atlas 1994* (NOAA Atlas NESDIS 4, Washington D.C.).

Ogilvy, J. A. (**1987**). "Wave scattering from rough surfaces," Rep. Prog. Phys. **50**, 1553–1608.

Park, M., Odom, R. I., and Soukup, D. J. (**2001**). "Modal scattering: A key to understanding oceanic T-waves," Geophys. Res. Lett. **28**, 3401–3404.

Stephen, R. A. (**2000**). "Optimum and standard beam widths for numerical modeling of interface scattering problems," J. Acoust. Soc. Am. **107**, 1095–1102.

Taflove, A., and Hagness, S. C. (**2000**). *Computational Electrodynamics: The Finite Difference Time-Domain Method* (Artech House, Boston).

Talandier, J., and Okal, E. A. (**1998**). "On the mechanism of conversion of seismic waves to and from T waves in the vicinity of Island Shores," Bull. Seismol. Soc. Am. **88**, 621–632.

Tolstoy, I., and Ewing, M. W. (**1950**). "The T phase of shallow focus earthquakes," Bull. Seismol. Soc. Am. **40**, 25–51.

Virieux, J. (**1986**). "P-SV wave propagation in heterogeneous media; Velocity-stress finite-difference method," Geophysics **51**, 889–901.